Heterointerface dipoles: Applications to (a) $Si-SiO_2$, (b) nitrided $Si-N-SiO_2$, and (c) $SiC-SiO_2$ interfaces

G. Lucovsky[a)]
Department of Physics, Department of Materials Science and Engineering, and Department of Electrical and Computer Engineering, North Carolina State University, Raleigh, North Carolina 27695-8202

H. Yang
Department of Chemistry, North Carolina State University, Raleigh, North Carolina 27695-8204

H. Z. Massoud
Department of Electrical Engineering, Duke University, Durham, North Carolina 27708-0291

(Received 21 January 1998; accepted 21 May 1998)

This article identifies procedures to calculate charge-transfer dipoles at semiconductor–dielectric interfaces, focusing primarily on the $Si-SiO_2$ system. Since SiO_2 is more polar than Si, there is a transfer of electrons from Si to SiO_2 to balance the difference in chemical potentials creating a dipole localized at the semiconductor–dielectric interface. This dipole increases the conduction-band offset energy difference between Si and SiO_2, and therefore, has important effects on interface electrical and optical properties. Empirical chemistry and *ab initio* methods have been applied to molecular clusters which emulate the interface bonding, and have been used to calculate interfacial charge transfer at (i) abrupt $Si-SiO_2$ interfaces and (ii) nitrided $Si-N-SiO_2$ interfaces. Additional calculations have applied to determine the average dipoles at $Si-SiO_2$ interfaces with suboxide bonding in excess of the monolayer level required to form an ideal interface. The calculations support experimental data that indicate that the effective conduction-band offset energies at nitrided $Si-N-SiO_2$ interfaces and at interfaces with minimized suboxide bonding are essentially the same. Finally, the calculations have been extended to $SiC-SiO_2$ interfaces to illustrate the effects of changing from a homopolar to a more ionic or heteropolar semiconductor.
© *1998 American Vacuum Society.* [S0734-211X(98)07604-5]

I. INTRODUCTION

The energy difference (or offset) between the conduction bands of crystalline Si and the SiO_2 gate dielectric in metal–oxide–semiconductor (MOS) field-effect transistors (FETs) plays a significant role in determining many optical and electrical properties including the barrier heights for internal photoemission and electrical tunneling, and the threshold voltages which define the onset of current flow in *n*-channel FETs. Similar considerations also apply for the valence-band offset energies. As FET device dimensions shrink in the deep submicron (e.g., channel lengths $<0.15\ \mu m$), the oxide equivalent thickness of gate dielectrics must be reduced proportionally to less than 3 nm, a thickness regime in which direct tunneling can play a significant role in the off-state leakage current.[1] Benefits of nitridation of ultrathin oxides have been identified, and include (i) decreased defect generation under accelerated stress bias testing, (ii) decreased Fowler–Nordheim and direct tunneling currents, and (iii) containment of boron penetration out of heavily doped p^+ polycrystalline gate electrodes.[2–4] The first two improvements are associated with interface nitridation at the monolayer level,[2,3] whereas the third is optimized by plasma-assisted top surface nitridation,[3] or the use of stacked oxide-nitride (ON) dual-layer dielectrics.[4] This article addresses one aspect of interface nitridation by comparing charge-transfer dipoles at nitrided and non-nitrided $Si-SiO_2$ interfaces.

The driving force for the charge-transfer process underlying the results of this article was identified more than ten years ago.[5–7] At that time, it was shown that equalization of the chemical potential across the interface layer was responsible for interfacial charge transfer. The chemical-potential equalization process was quantified using an empirical approach by applying the principal of electronegativity equalization as formulated by Sanderson.[8–10] The motivation for the analysis in Ref. 7 was to explain differences in the sign of the valence-band offset energies for $Si-SiO_2$ interfaces that had been hydrogenated or cesiated. The motivation in Refs. 8 and 9 was to explain differences between flatband voltages at $Si(111)-SiO_2$ and $Si(100)-SiO_2$ interfaces. The major contribution of this article is to go significantly beyond the *zeroth-order* model calculations of Refs. 7–9, and develop a more quantitative approach that could be applied to (i) nitrided $Si-N-SiO_2$ interfaces, (ii) $Si-SiO_2$ interfaces with suboxide transition regions, as well as (iii) other semiconductor dielectric interfaces such as $SiC-SiO_2$. In addition, the success of this model in addressing nitrided $Si-N-SiO_2$ and $Si-SiO_2$ interfaces with suboxide transition regions has provided an important perspective with respect to the different roles that interface nitridation and suboxide transitions regions play in strain relief at $Si-SiO_2$ interfaces.

a)Electronic mail: gerry_lucovsky@ncsu.edu

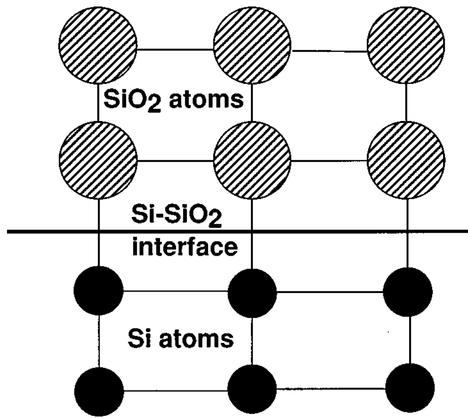

FIG. 1. Molecular model for abrupt interfaces between Si(111) and SiO_2 ''atoms.''

The approach of Refs. 8–10 is reviewed to provide a background for development of the calculations of this article. The Sanderson electronegativity approach uses an empirically based method for determining charge transfer between near-neighbor atoms with different electronegativities.[8–10] Figure 1 indicates the simplified structural model of Refs. 6 and 7 as it was first applied to abrupt Si(111)–SiO_2 interfaces. The calculation of the charge-transfer dipole was performed at a *molecular level* where the two *molecular constituents* were the Si atoms of the crystalline substrate and SiO_2 *pseudoatoms* of the oxide layer. The driving force for interfacial charge transfer is the electronegativity equalization principle of Refs. 8–10. If S_A is the electronegativity of one atom of a diatomic molecule AB, and S_B the electronegativity of the other atom, then charge is transferred between A and B until they reach the same electronegativity or chemical potential. A geometric mean is used to define electronegativity equalization, so that if S_A^* and S_B^* are the equalized atomic electronegativities after charge transfer has occurred, then $S_A^* = S_B^* = (S_A \times S_B)^{0.5}$. This approach has been extended to larger molecules in which the atoms have additional nearest, and/or more distant neighbors.[11] Once the values of S_A^* and S_B^* have been determined, partial charges on A and B, e_{pA}, and e_{pB}, respectively, can be calculated using an empirical relationship developed in Refs. 8–10,

$$e_{pA} = (S_A^* - S_A)/0.8 \times S_A^{0.5}$$

and

$$e_{pB} = (S_B^* - S_B)/20.8 \times S_B^{0.5}, \qquad (1)$$

where the normalization constant in the denominator is based on an assumed ionicity of 75% for the NaF molecule. If A has lower electronegativity, the partial charge of A is positive and the partial charge of B is negative, indicating a direction of charge transfer consistent with the definition of electronegativity as first proposed by Pauling.[12]

Applying the diatomic molecule model to the Si–SiO_2 interface in Fig. 1, the renormalized electronegativities after chemical-potential equalization are 3.85 for both Si and SiO_2, yielding partial charges of $+0.18\ e$ for Si and $-0.18\ e$ for SiO_2. If a less ''electronegative'' dielectric such as Si_3N_4 is substituted for SiO_2, then the renormalized electronegativities are smaller, leading to reduced partial charges of +0.11 for Si and −0.11 for Si_3N_4. Applied to Si–SiO_2 interfaces in MOS structures, the molecular model of Refs. 6 and 7 has yielded charge-transfer dipoles that account for differences in flatband voltages reported for MOS devices on Si(100) and Si(111) substrates.[6,7] In Refs. 6 and 7 a *road map* was presented for extending the electronegativity equalization approach to more complicated interfaces such as those that include interfacial nitridation, and/or interfacial suboxide bonding. This article follows that *road map* and focuses on interfacial bonding issues that have emerged as being important at Si–SiO_2 interfaces with ultrathin oxide dielectrics and nitrided interfaces.

TABLE I. Calculated charges, dipole moments, and dipole potential steps for Si(111) interfaces.

Interface bonding	Partial charge on Si ±0.01 (e)	Dipole moment ±0.01 ($e \times$Å)	Potential step ±0.01 (eV)
(a) Abrupt Si–SiO_2			
Two-layer	0.18	0.29	0.54
Empirical cluster	0.23	0.37	0.67
Ab initio cluster	0.22	0.36	0.68
(b) Nitrided Si–N–SiO_2			
Two-layer	0.15	0.26	0.48
Empirical cluster	0.18	0.31	0.57
Ab initio cluster	0.18	0.36	0.65
(c) Si–SiO_x–SiO_2			
Two-layer	0.16	0.25	0.47
Empirical cluster	0.17	0.28	0.52
Ab initio cluster	0.18	0.29	0.54
(d) Abrupt Si–Si_3O_4			
Two-layer	0.11	0.20	0.30
Empirical cluster	0.14	0.24	0.36

II. CALCULATIONS OF CHARGE-TRANSFER INTERFACE DIPOLES

Charge-transfer dipoles are calculated in two different ways in this article: (i) by applying the empirical chemical method of Refs. 5–7 to larger clusters, which include the effects of more distant neighbors in a manner consistent with the approaches previously developed for large molecules[11,13] and disordered networks;[14,15] and (ii) by using hydrogen-terminated molecular clusters as discussed in Ref. 16. These results are then compared in Table I with the results calculated from the ''pseudomolecule'' approach of Refs. 6 and 7. In order to make these comparisons, it was necessary to extend the approach of Refs. 6 and 7 to include monolayer interface nitridation and suboxide transition regions. For the nitrided interface, the ''pseudomolecule'' that was used to replace SiO_2 in Fig. 1 was characterized by the average electronegativity of SiO_2 and Si_3N_4, 3.63. This gives a Si-atom partial charge of 0.15 e, as compared to 0.18 e for the Si–SiO_2 interface. Similarly, for the interface with a subox-

ide transition region, the ''pseudomolecule'' that was used to replace SiO_2 in Fig. 1 was characterized by the average electronegativity of SiO_2 and SiO, 3.85, yielding a Si-atom partial charge of 0.16 *e*. Since the Si–N bond length is about 7% larger than the Si–O, this calculation gives essentially equal interfacial dipole moments of about 0.25 *e* Å.

Consider next the empirical chemical approach. As noted above, the computational basis for including near-nearest- and more-remote-neighbor chemical induction effects in molecules was first developed by Carver and Gray.[11] This was subsequently extended by Lucovsky and co-workers to network amorphous solids.[14,15] Using the method of Ref. 14, the interface between crystalline Si oriented in a (111) direction, and noncrystalline SiO_2 is represented by the molecular cluster in Fig. 2(a). The Si side of the cluster consists of a three atomic shells (two are shown in the diagram): (i) the Si atom at the *interface* in shell (1), (ii) the three nearest-neighbor Si atoms in shell (2), and (iii) nine pseudoatoms in shell (3), which are characterized by the average electronegativity of the rest of the network. A similar construction is used for the SiO_2 network on the other side of the interface. In this case, the cluster contains atomic shells of alternating Si and O atoms, as well as a final shell that is comprised of pseudoatoms with the average electronegativity of the SiO_2 network ($S_{\text{average}}=[(S_{\text{Si}})(\text{Si}_{\text{O}})^2]^{1/3}=4.26$). A similar cluster has been used for the *ab initio* calculations, except that the terminating species are hydrogen atoms rather than *pseudoatoms* with average properties. The cluster used for empirical calculations as applied to abrupt nitrided Si–N–SiO_2 interfaces is shown in Fig. 2(b). It is not possible to characterize suboxide bonding by a single representative cluster. In order to illustrate the effects of suboxide bonding it is, therefore, reasonable to average over two clusters that emulate an average SiO composition. This is done by combining the cluster in Fig. 2(a) for the idealized Si–SiO_2 interface with the cluster in Fig. 2(c), which effectively extends the Si substrate into oxide and increases the coordination of the interface Si atom of the substrate with oxygen atoms from one to three.

Total energy *ab initio* calculations were performed using a many-electron embedding theory that permits accurate computation of molecule–solid-surface interactions. Calculations were carried out at an *ab initio* configuration interaction (CI) level, in which all electron–electron interactions are explicitly calculated and there are no exchange approximations or empirical parameters. The details of the method are extensively discussed in Refs. 17–19. The *ab initio* calculations are performed by first obtaining self-consistent-field (SCF) solutions for the H-atom-terminated dielectric and Si substrate clusters. The occupied and virtual orbitals of the SCF solution are then transformed separately to obtain orbitals spatially localized within the bonds of the dielectric cluster and the Si substrate. This unitary transformation of orbitals, which is based upon exchange maximization with atomic valence orbitals, enhances convergence of the configuration interaction expansion.[17–19]

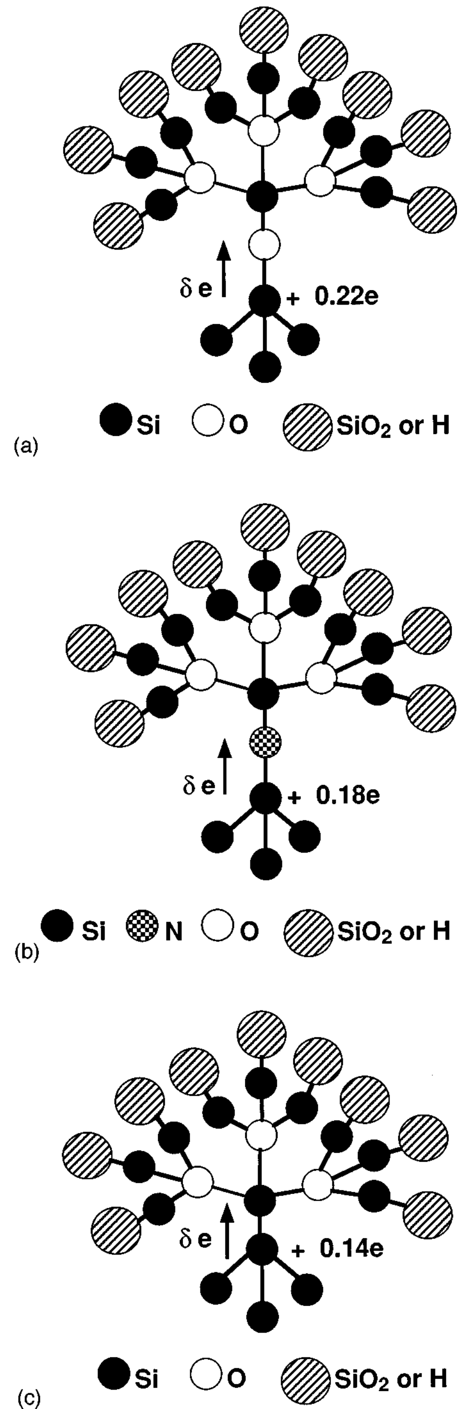

FIG. 2. Cluster model for Si–dielectric interfaces: (a) abrupt Si(111)–SiO_2, (b) abrupt nitrided Si(111)–N–SiO_2, and (c) Si(111)–SiO_2 with interfacial transition region with suboxide transition region. The dipole charges in this figure are from the *ab initio* calculations.

III. RESULTS

Table I includes the results of the three calculations described above. Presented in Table I are: (i) the partial charge on the substrate Si atom, (ii) the charge-transfer dipole, and (iii) the calculated potential step at the interface. The potential step ΔV was obtained using the approach of Refs. 6 and 7, i.e.,

$$\Delta V=[e_{p\mathrm{Si}}\times l_d\times N_{\mathrm{Si}}(111)\times\sin\Phi/(\epsilon_{\mathrm{AV}})],\tag{2}$$

where l_d is the atomic separation between the Si atom of the substrate and the first atomic shell of the dielectric, $N_{\mathrm{Si}}(111)$ is the areal density of Si atoms on a Si(111) surface, Φ the angle between the substrate Si-atom bond and the interface, and e_{AV} is an average dielectric constant, e.g., $e_{\mathrm{AV}}=(e_{\mathrm{Si}}+e_{\mathrm{SiO_2}})/2=7.75$.

Consider first the abrupt Si(111)–SiO_2 interface. The empirical two-layer molecular model of Refs. 6 and 7 gives values of $e_{p\mathrm{Si}}$ and ΔV that are smaller, respectively, than those obtained by the cluster calculations approaches. In addition, the value of ΔV is less than that given in Refs. 6 and 7 due to the assumption of different charge separation dipole distances. In the calculations of this article, a nominal Si–O bond length of 0.162 nm (1.62 A) was used, whereas the calculations of Refs. 6 and 7 employed a larger value that was estimated from the covalent bonding radius of Si and the ''size'' of a SiO_2 ''molecule.'' More importantly, the empirical calculations and the *ab initio* calculations based on the cluster structures of this article [see Fig. 2(a)] give essentially the same results for the partial charge and the interface potential step at abrupt Si–SiO_2 interfaces. For the empirical calculation, the nominal dipole length of 0.162 nm was used in calculating ΔV, whereas for the *ab initio* approach, the ~3% larger relaxed Si–O bond length of the energy optimization calculation was used. Based on an electron energy representation of the interface band structure, the direction of the dipole increases the potential step at the conduction-band discontinuity between the Si(111) substrate and the SiO_2 conduction band. This would lead to negative shifts of the flatband and threshold voltages in MOS devices.[6,7]

Similar results were obtained using the cluster in Fig. 2(b) for an abrupt N-atom-terminated interface Si–N–SiO_2. As displayed in Table I, the *diatomic molecular model* of Refs. 6 and 7 gives values of $e_{p\mathrm{Si}}$ and ΔV that are again smaller than those obtained by the cluster calculations of this article. However, as the case of the Si–SiO_2 calculations, the empirical and *ab initio* calculations based on the cluster model of this article give essentially the same results for the partial charge and the interface potential steps. The difference between the nominal Si–N bond length of 0.174 nm, and the one obtained in the *ab initio* calculation accounts for the differences in ΔV between these calculations. The significant result of these calculations on nitrided Si–SiO_2 interfaces is that the partial charge on the Si atom of the substrate is reduced by the interposition of a N atoms at Si–SiO_2 interfaces, and that this leads to a small reduction of the interface potential step of approximately 0.1 eV with respect to non-nitrided abrupt Si–SiO_2 interfaces. To confirm the trends in $e_{p\mathrm{Si}}$ and ΔV for interface nitridation, calculations based on the *molecular model* of Refs. 6 and 7, and the empirical cluster model of this article were performed for a Si(111)–Si_3N_4 interface, and these have also been included in Table I. These calculations support the differences obtained for the abrupt Si(111)–SiO_2 and nitrided Si(111)–N–SiO_2 interfaces, since increased nitridation leads to smaller interfacial dipoles with correspondingly smaller contributions to the conduction-band offset energies.

Finally, Table I includes the results of calculations for Si(111)–SiO_x–SiO_2 interfaces with suboxide transitions regions. Different degrees of suboxide bonding have been approximated by placing a Si atom in the first shell of the dielectric and then increasing the number of Si atoms in the second shell bonded to that atom [see Fig. 2(c)]. As the number of Si atoms in the second shell increases, the partial charge on the Si atom of the substrate decreases, and the potential step contribution ΔV also decreases proportionally. However, the *ab initio* calculation for this type of interface was performed for the cluster with only one layer of suboxide bonding with no additional Si atoms attached to the Si atom of the first shell of the transition region. For purposes of comparison, the entries into Table I for the interface with suboxide bonding, Si(111)–SiO_x–SiO_2, are the average of the results obtained for the clusters in Figs. 2(a) and 2(c).

The charge transfer interface dipole has been calculated as a function of the interatomic distance of the interface atoms, i.e., the Si–O distance as in Fig. 2(a), Si–N distance as in Fig. 2(b), and Si–Si distance as in Fig. 2(c), and these results are presented in Figs. 3(a), 3(b), and 3(c). The results in Figs. 3(a) and 3(b) for the clusters of Figs. 2(a) and 2(b), respectively, demonstrate that the charge-transfer dipole decreases approximately linearly with increasing interatomic distance for the abrupt Si–SiO_2 and nitrided Si–N–SiO_2 interfaces. This dependence of the charge-transfer dipoles requires that the partial charge on the Si atom decrease approximately quadradically with increasing interatomic spacing for the range of the interfacial bond lengths explored. In contrast and as shown in Fig. 3(c), the variation of the charge-transfer dipole with interface bond length is reversed for the cluster that is used to emulate suboxide bonding so that the dipole increases with increasing Si–Si separation. Analysis of this dependence shows that it is a direct consequence of competition between two different contributions to the interface dipole. One contribution comes from a dipole between the Si substrate atom and the Si atom of the first shell of the dielectric that is directed toward the Si substrate, and the second contribution that is oppositely directed comes from the atoms of the second and third shells of the dielectric. The net effect of these two contributions is to give an effective interfacial dipole that is significantly smaller than that of an abrupt Si(111)–SiO_2 interface. This explanation is supported in Fig. 3(c) by an additional observation that shows that as the Si–Si distance is increased out of a linear regime the value of the interfacial charge-transfer dipole approaches the value of the dipole expected for a Si–SiO_2 bonding arrangement.

The calculations of this article have been extended to Si(100)–SiO_2 interfaces for the empirical cluster calculation method, and the results of the these calculations are presented in Table II. In all instances the partial charge on the Si(100)-substrate atom is increased, but the dipole, and hence, the potential step are decreased. The increase in partial charge is due to the increase in the number of bonding connections per Si interface atom (from one to two) to the

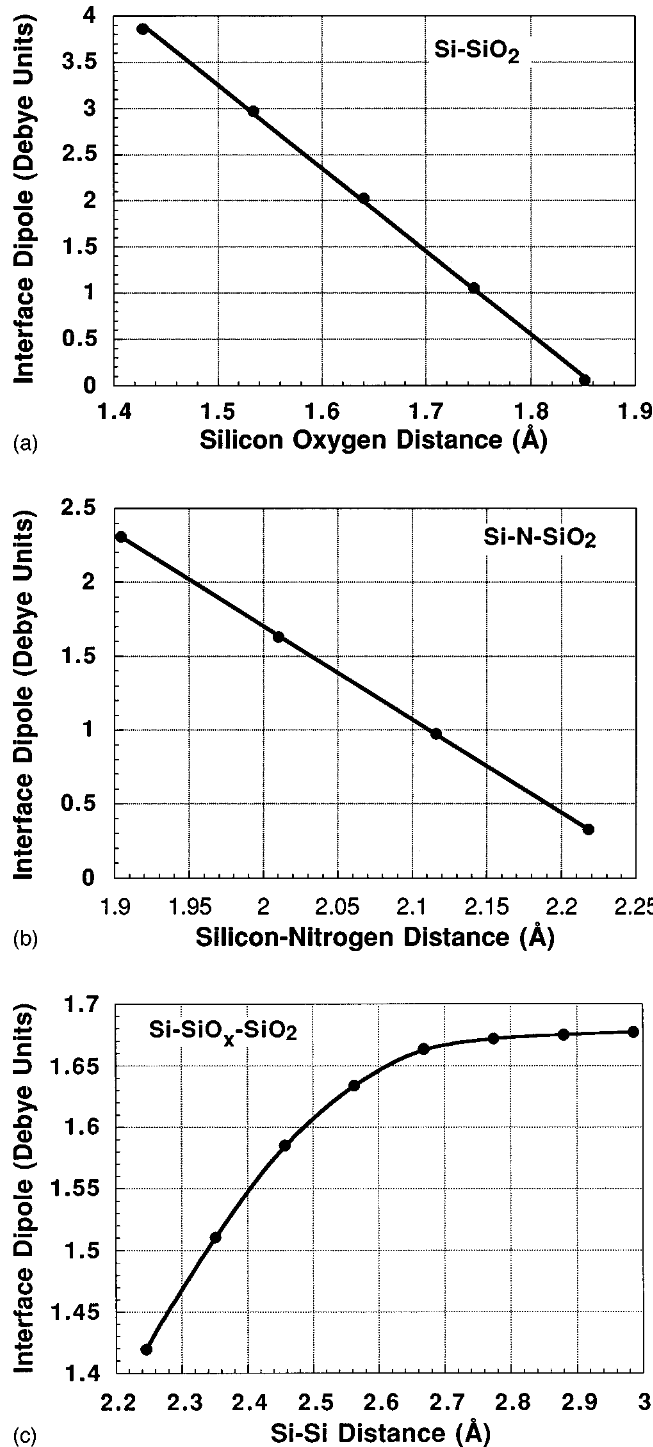

FIG. 3. Interface dipole as a function of interface bonding distance from the abate calculations: (a) abrupt Si(111)–SiO_2, (b) abrupt nitrided Si(111)–N–SiO_2, and (c) Si(111)–SiO_2, with interfacial transition region with suboxide transition. The solid lines in (a) and (b) are a linear fit to the calculated data points; the solid line in (c) is a smooth fit to the calculated data points.

dielectric, and the decrease in the potential step is due to the bonding geometry. In particular, the sin Φ factor is reduced from 1 to 0.577 as the projection angle of the dipole onto a normal to the plane of the interface decreases from 90° to 35.25°.

TABLE II. Calculated charges, dipole moments, and dipole potential steps for Si(100) interfaces.

Interface bonding	Partial charge on Si ±0.01 (e)	Dipole moment ±0.01 (e×Å)	Potential step ±0.03 (eV)
(a) Abrupt Si–SiO_2			
Empirical cluster	0.32	0.28	0.46
(b) Nitrided Si–N–SiO_2			
Empirical cluster	0.26	0.26	0.41
(c) Si–SiO_x–SiO_2			
Empirical cluster	0.21	0.24	0.38

Table III presents the results of empirical cluster calculations for SiC(0001)–SiO_2 interfaces. The major difference between the calculated partial charges on the Si atom on the SiC(0001) substrate and on the Si(111) substrate are driven by the heteropolar character of the SiC semiconductor. The increased polar character of the SiC substrate reduces the partial charge on the Si surface atom relative that of the Si(111) substrate.

IV. DISCUSSION

This section addresses several different aspects of the calculations of Sec. III including (i) development of a band model for the Si–SiO_2 interface that takes into account differences due to interface nitridation, and interfacial suboxide regions; (ii) the comparison of these calculations with experimental results for Si–SiO_2 interfaces; and (iii) a perspective for semiconductor dielectric interfaces that parallels a framework established for lattice-mismatched semiconductor–semiconductor heterointerfaces.

A. Band model for Si–SiO_2 interfaces

Figure 4 presents a band model for the conduction- and valence-band offset energies between Si and SiO_2. As shown in the diagram, there are two contributions to the conduction-band (and therefore, also the valence-band) potential steps: (i) the first comes from differences between the potential steps of the respective interface components relative to

TABLE III. Comparisons of partial charges on Si interface atoms between Si(111) and Si-atom terminated SiC(0001) interfaces.

Interface bonding	Partial charge on Si	
	Si(111) ±0.01 (e)	SiC(0001) ±0.01 (e)
(a) Abrupt Si–SiO_2		
Two-layer	0.18	0.13
Empirical cluster	0.23	0.17
(b) Nitrided Si–N–SiO_2		
Two-layer	0.15	0.10
Empirical cluster	0.18	0.12
(c) Si–Si_3N_4		
Two-layer	0.11	0.06
Empirical cluster	0.14	0.08

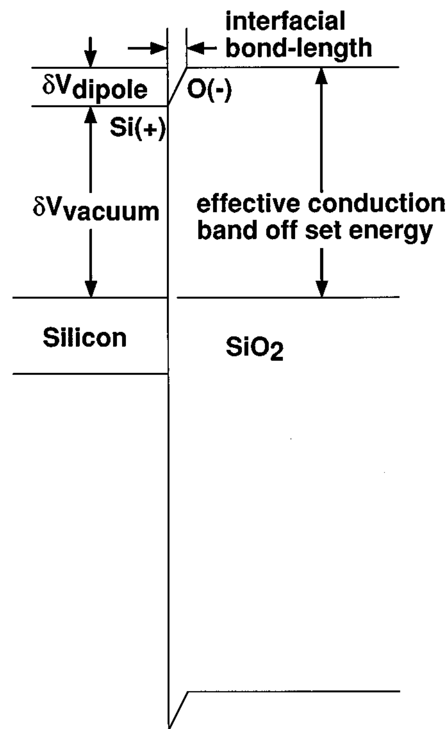

FIG. 4. Band model for Si–SiO_2 interfaces show interface potential due to charge-transfer dipoles.

vacuum, and (ii) the second comes from the interfacial dipoles of this article. DiMaria and co-workers performed internal photoemission measurements to determine the conduction-band potential steps between Si and SiO_2 (Ref. 20) and Si and Si_3N_4,[21] and these values have been used extensively in characterizing interface properties, as for example, in calculations of direct tunneling currents.[22] The results of this article indicate that care must be taken in applying these nominal conduction-band offset potential-energy steps. For example, the calculations of this article have demonstrated significant differences in effective conduction-band offset energies that depend on the local atomic bonding at the interface, including both interface nitridation, and transition regions with suboxide bonding.

B. Comparison with experiments

The calculations of this article are now compared with results of several different experimental studies. First, a word of caution regarding such comparisons. There are two factors involved in interface formation that contribute to differences in interfacial bonding arrangements of the types discussed in this article: (i) the process, or process steps by which the interface is formed, as for example, thermal oxidation, plasma-assisted oxidation, plasma-assisted oxidation combined with post-oxidation nitridation, etc., and (ii) the chemical and structural interfacial relaxations associated with post-formation rapid thermal annealing (RTA), or downstream thermal exposures. The combination of these two interface fabrication effects is illustrated by results obtained from optical second-harmonic-generation (SHG) experiments on vicinal Si(111)–SiO_2 interfaces,[23–25] which are presented in Table IV.

TABLE IV. Summary of results from studies of vicinal Si(111) surfaces off-cut ~5° in the 112 bar direction.

(a) Surface treatment—plasma processing[a]	Phase: $\Delta\Phi_{13}$ ±2°	A_1/A_3 ±0.03
O_2, 15 s, 300 °C	68	0.20
O_2, 15 s, 30 s 900 °C RTA (0.5%O_2/Ar)[b]	23	0.35
N_2O, 15 s, 300 °C	67	0.21
N_2O, 15 s, 30 s 900 °C RTA (Ar)	11	0.37
N_2O, 30 s, 300 °C	65	0.17
N_2O, 30 s, 30 s 900 °C RTA (Ar)[b]	11	0.35
(b) Surface treatment—thermally grown interfaces		
Furnace oxidation at 850 °C	72	0.19
Postoxidation anneal (30 s at 950 °C (0.5%O_2/Ar)	23	0.33

[a]Predeposition remote plasma-assisted oxidation step.
[b]Processing conditions for optimum electrical properties.

The experimental approach and the data reduction procedures for the optical SHG studies are described in detail in Refs. 23 and 24. The columns in Table IV labeled A_1/A_3 and $\Delta\Phi_{13}$, which are obtained from a harmonic analysis of angular anisotropy measurements in vicinal Si(111) surfaces and reflect differences in interface bonding as a function of the two processing factors identified above. The SHG response is dominated by the Si–SiO_2 interface for the polarizations of the incident and reflected optical waves at ω and 2ω, respectively. Combined with the results presented in Ref. 26, which demonstrate significant reductions in interfacial transition regions following a 30 s 900 °C RTA in a chemically inert ambient such as Ar or He, the SHG results in Table IV demonstrate that interfaces formed by thermal oxidation at temperatures below 850 °C, and remote plasma-assisted oxidation/nitridation at 300 °C, display the same values of A_1/A_3 and $\Delta\Phi_{13}$, and are essentially the same with suboxide transition regions being the determinant factor in determining interface properties. After the anneal, the non-nitrided interfaces formed by either thermal or remote plasma-assisted oxidation are essentially the same, but are different from the interfaces that contain approximately 1 monolayer (ML) of interface nitridation. X-ray photoelectron spectroscopy (XPS) studies on non-nitrided interfaces have established that (i) there is a reduction of suboxide bonding following the 30 s 900 °C RTA for non-nitrided interfaces formed by both thermal and plasma-assisted oxidation, and (ii) following the RTA, there is still measurable suboxide bonding ~1.5 excess monolayer equivalents of suboxide bonded Si atoms, as opposed to approximately 3 ML equivalents before RTA.[27]

In the examples that are discussed below, the Si–SiO_2 interfaces were subjected to a 30 s 900 °C RTA so that comparisons between the calculations and experiment will utilize the results of the *ab initio* calculations for the abrupt nitrided Si–SiO_2, and the interface with the smallest amount of sub-

oxide bonding. The interfaces characterized by optical SHG have been prepared on Si(111) surfaces, where as those discussed below for MOS devices were formed on Si(100) substrates. It was established earlier in Tables I and II that qualitative trends in interface potential steps as a function of interface bonding are the same for Si(111) and Si(100) interfaces. The differences are in the quantitative aspects of the calculations, namely, the magnitudes of the ΔVs, and differences in these values for different interface bonding on Si(111) and Si(100) substrates are small and within the experimental uncertainties of the experimental data.

It is tempting to compare the results of these calculations with barrier heights used to interpret tunneling studies on MOS devices with ultrathin gate dielectrics; however, the extraction of effective barrier heights from tunneling data is not unambiguous. For example, it depends on assumptions made about the magnitude of the effective mass of the tunneling electrons, and approximations made taking into account potential drops in the substrate and polycrystalline gate electrodes.[22] The results presented in Ref. 28 demonstrate that tunneling current densities are markedly different for nitrided and non-nitrided interfaces with nitrided interfaces showing reductions in tunneling current that are independent of the direction of the injection, substrate, or gate, and that are also quantitatively the same for tunneling in the Fowler–Nordheim (5 nm) and direct tunneling (2 and 3 nm) regimes. However, since the flatband voltages vary by no more than 0.05 eV, the reductions in tunneling current are not due to deferences in barrier heights at the substrate–Si/dielectric layer interface. Since the samples in Ref. 28 were subjected to postdeposition annealing in inert ambients at 900 °C, this leads us to conclude that the effective barrier heights at structurally and chemical relaxed, nitrided, and non-nitrided interfaces are essentially the same. This suggests that the effective barrier height at Si–SiO_2 interfaces with minimal suboxide bonding is essentially the same are for a fully nitrided interface. This result is consistent with the calculations presented in Tables I and II. The agreement between the predictions of the calculation and the tunneling experiments validates the average bonding model used for the interfaces with minimal suboxide bonding.

C. Stress relief at Si–SiO_2 interfaces

The results presented in this article, and in particular, the good agreement between the calculations and the tunneling experiments provide an important insight into the issue of the different roles of suboxide bonding and interface nitridation in stress relief at Si–SiO_2 interfaces. There is a large molar volume mismatch between Si and SiO_2 that means that the effective spacing of Si atoms in these two materials is markedly different. The Si–Si bond length in crystalline Si is 0.235 nm (2.35 A), whereas the second-nearest-neighbor Si–Si distance in SiO_2 is 0.305 ± 0.005 nm (3.05 ± 0.05 Å). The large mismatch in interatomic distances means that the Si–SiO_2 interface is in many respects an analog of lattice-mismatched semiconductor heterointerfaces. The formation of non-lattice-matched semiconductor heterointerfaces is accomplished in several different ways: (i) by pseudomorphic growth habits, where there are large strains in the epitaxial overgrowth layer and wherein the maximum thickness of the pseudomorphic overgrowth is inversely proportional to the strain; (ii) by the formation of interface defects in the form of dislocations; and (iii) by reduction of interface strain through the use of buffer layers with intermediate values of lattice constants.

The formation of non-nitrided Si–SiO_2 interfaces requires a transition region with suboxide bonding to reduce the very large strain mismatch between the Si and the SiO_2. From the XPS studies, it can be concluded that the minimum suboxide bonding region after postoxidation annealing at 900 °C contains about 1.5 ML of Si.[27] The incorporation of interfacial nitrogen at the monolayer level is an analog of the buffer layer approach, where a material with a different composition can accommodate a significant fraction of the strain mismatch and thereby reduce the strain and require reduced suboxide bonding.

Strain is developed differently at interfaces formed in different ways. For example, it has been shown that Si–SiO_2 interfaces with relatively thick oxide layers (>50 nm) formed by conventional thermal oxidation in dry O_2, display very nearly uniform levels of compressive stress in the oxide regions, thereby being analogous to pseudomorphic semiconductor–semiconductor heterostructures. Additional experiments have demonstrated strain relief in these oxides at annealing temperatures greater than or equal to about 1000 °C. After such anneals, there is a considerable strain gradient in the oxide layers extending to distances of approximately 20 nm. Finally, strain is pinned at the Si–SiO_2 interface at a level that corresponds to ~0.002–0.003.[29] Recent experiments on significantly thinner oxides, <50 nm, have identified transition regions and interfaces formed in this way, and additionally at interfaces formed by remote plasma-assisted oxidation.[26] This leads us to conclude that one class of optimally relaxed interfaces contain a relatively thin transition region between the Si substrate and SiO_2 layer in which the excess concentration of Si atoms with suboxide bonding is of the order of 1.5 ML. Oxides under about 100 nm do not appear to support significantly strain, and interface chemical and mechanical strain appear to be completely relaxed by the 900 °C RTAs discussed above. Finally, a monolayer of interfacial N atoms at Si–SiO_2 interfaces provides an alternative pathway for interface relaxation paralleling the introduction of graded strain relief layers in semiconductor–semiconductor heterostructures. As discussed in other publications, the preferential bonding of nitrogen atoms at Si–SiO_2 interfaces is determined by three factors.[30] The Si–N bond energy is estimated to be about 0.3 eV smaller than the Si–O bond energy. However, the mechanical and chemical strain produced by nitrogen atom bonding to Si atoms are both less than the corresponding Si–O strain energies. The preferential bonding of nitrogen means that the decrease in these strain energies more than compensates for the difference in bond energies.

V. SUMMARY

In summary, this article has demonstrated that interfacial transition regions at non-nitrided Si–SiO_2 interfaces reduce the partial charge of Si atoms on the *Si side* of that interface, thereby reducing the interfacial charge-transfer dipole below the value it would have for an abrupt Si–SiO_2 interface with no suboxide bonding beyond what is required to define the interface. Monolayer concentrations of nitrogen atoms incorporated at Si–SiO_2 interfaces have a similar effect in the context that they also reduce the partial charge on the Si atoms on the Si side of the interface below the value it would have had at an abrupt Si–SiO_2 interface. The model calculations based on empirical chemistry and *ab initio* approaches applied to the same interface cluster models, combined with the two-layer molecular approach indicate the conduction-band offset between Si and SiO_2 is only slightly increased by monolayer nitrogen-atom incorporation as compared to minimal suboxide bonding. For Si(111) interfaces, the calculated average difference in interfacial conduction-band offsets, $\delta\Delta V$, is estimated to be 0.05 ± 0.03 eV. Similar differences are obtained for Si(100) interfaces using the empirical cluster model. The results of recent experiments on tunneling currents in fully nitrided Si(100)–SiO_2 interfaces are in accord with the predictions of these calculations. The reduction in tunneling currents for nitrided interfaces reported in Ref. 29 must then be attributed to other factors including, for example, reductions in interface roughness that accompany interfacial nitridation.

ACKNOWLEDGMENTS

This research is supported by the Office of Naval Research (ONR), the National Science Foundation (NSF) Engineering Research Center (ERC) at North Carolina State University (NCSU), and the Semiconductor Research Corporation (SRC).

[1] D. Buchanan, J. Vac. Sci. Technol. B (to be published).
[2] D. R. Lee, G. Lucovsky, M. R. Denker, and C. Magee, J. Vac. Sci. Technol. A **13**, 1671 (1995); D. R. Lee, C. R. Parker, J. R. Hauser, and G. Lucovsky, J. Vac. Sci. Technol. B **13**, 1778 (1995).
[3] S. V. Hattangady *et al.*, Tech. Dig. Int. Electron Devices Meet., 495 (1996).
[4] Y. Wu, G. Lucovsky, and H. Z. Massoud, in Proc. IEEE Reliability Phys. Symp. (1998).
[5] P. Perfetti, C. Quaresima, C. Coluzza, C. Fortunato, and G. Margaritondo, Phys. Rev. Lett. **57**, 2065 (1986).
[6] H. Z. Massoud, Mater. Res. Soc. Symp. Proc. **105**, 265 (1988).
[7] H. Z. Massoud, J. Appl. Phys. **63**, 2000 (1988).
[8] R. T. Sanderson, *Chemical Periodicity* (Van Nostrand Reinhold, Princeton, NJ, 1960).
[9] R. T. Sanderson, *Inorganic Chemistry* (Reinhold, New York, 1967).
[10] R. T. Sanderson, *Chemical Bonds and Bond Energy*, 2nd ed. (Academic, New York, 1976).
[11] J. C. Carver, R. C. Gray, and D. M. Hercules, J. Am. Chem. Soc. **96**, 6851 (1984).
[12] L. Pauling, *The Nature of the Chemical Bond*, 3rd. ed. (Cornell University Press, Ithaca, NY, 1960).
[13] G. Lucovsky, Solid State Commun. **29**, 571 (1979).
[14] D. V. Tsu, B. N. Davidson, and G. Lucovsky, Phys. Rev. B **40**, 1795 (1989).
[15] G. N. Parsons and G. Lucovsky, Phys. Rev. B **41**, 1664 (1990).
[16] Z. Jing, G. Lucovsky, and J. L. Whitten, J. Vac. Sci. Technol. B **13**, 1613 (1995).
[17] P. Cremaschi and J. L. Whitten, Theor. Chim. Acta **72**, 485 (1987).
[18] J. L. Whitten and H. Yang, Int. J. Quantum Chem., Quantum Chem. Symp. **29**, 41 (1995).
[19] J. L. Whitten and H. Yang, Surf. Sci. Rep. **24**, 55 (1996).
[20] D. J. DiMaria, J. Appl. Phys. **50**, 5826 (1979).
[21] D. J. DiMaria (private communication).
[22] H. Y. Yang, H. Niimi, and G. Lucovsky, J. Appl. Phys. **83**, 2327 (1998).
[23] C. H. Bjorkman, T. Yasuda, C. E. Shearon, Jr., U. Emmerichs, C. Meyer, K. Leo, and H. Kurz, J. Vac. Sci. Technol. B **11**, 1521 (1993).
[24] C. H. Bjorkman, C. E. Shearon, Jr., Y. Ma, T. Yasuda, G. Lucovsky, U. Emmerichs, C. Meyer, K. Leo, and H. Kurz, J. Vac. Sci. Technol. A **11**, 964 (1993).
[25] U. Emmerichs, C. Meyer, H. J. Bakker, F. Wolter, H. Kurz, G. Lucovsky, C. Bjorkman, T. Yasuda, Yi Ma, Z. Jing, and J. L. Whitten, J. Vac. Sci. Technol. B **12**, 2484 (1994).
[26] G. Lucovsky, A. Banerjee, B. Hinds, B. Claflin, K. Koh, and H. Yang, J. Vac. Sci. Technol. B **15**, 1074 (1997).
[27] J. Rowe (unpublished).
[28] G. Lucovsky, H. Niimi, Y. Wu, C. G. Parker, and J. R. Hauser, J. Vac. Sci. Technol. A **16**, 172 (1998).
[29] C. H. Bjorkman, J. T. Fitch, and G. Lucovsky, Appl. Phys. Lett. **56**, 1983 (1990).
[30] K. Koh, H. Niimi, G. Lucovsky, and M. L. Green, Jpn. J. Appl. Phys. **83**, 2327 (1998).